Isospin Dependence of Proton and Neutron Radii within Relativistic Mean Field Theory *

M. Warda, B. Nerlo-Pomorska and K. Pomorski
Theoretical Physics Department, University M.C.S., Lublin, Poland

Abstract

The binding energies, shapes and sizes of even-even β–stable nuclei with $A \geq 40$ and a few chains of isotopes with Z=50, 56, 82, 94 protons and isotones with N=50, 82, 126 neutrons are analyzed. The average isospin dependence of the radii of protons and neutrons evaluated within the relativistic mean field theory is studied. A simple, phenomenological formula for neutron radii is proposed.

PACS numbers: 21.60.-n, 11.10.Ef, 21.10.Ft, 21.10.Gv, 21.10.Dr
Keywords: even-even nuclei, proton, neutron and charge radii, quadrupole moments, separation energies, binding energies

1 Introduction

The nuclear radii are ones of the crucial quantities good for testing of every theoretical model of nucleus. The radii are measured with a high accuracy for the charge density distributions [1] and less precise for the neutron ones [2]. The data concerning nuclear sizes and shapes are already known for many nuclei, especially for those close to the β stability line, but also more exotic nuclei are explored extensively by experimentalists at present. It would be worthwhile to know what the relativistic mean field theory (RMFT) predicts for such nuclei and to approximate the results in terms of a simple, practical formulae for radii.

The nuclear radii depend chiefly on the number of nucleons (A) [3]

$$R_0 = r_0 A^{1/3} \ , \tag{1}$$

where the radius constant r_0 ≈1.2 fm. It is the result of saturation property of nuclear forces which is manifested in the experimental fact that the volume of nucleus is roughly proportional to the mass number A. However, the formula (1) is not valid any more for nuclei in which numbers of protons (Z) and neutrons (N) differ significantly.

*This work is partly supported by the Polish Committee of Scientific Research under Contract No. 2 P03B 049 09.

It was found in Ref. [4] that the isospin dependent formula for the nuclear charge radius constant

$$r_0^{ch} = 1.25 \left(1 - 0.2 \cdot \frac{N-Z}{A}\right) \text{ fm}\,, \tag{2}$$

describes much better than Eq. (1) the experimentally known charge mean square radii of even-even nuclei with $A \geq 60$. The formula (2) was obtained assuming the uniform charge distribution within deformed nucleus. In such an approximation the root mean square radius (RMSR) of deformed nucleus is given by the following formula

$$< r^2 >^{1/2} = \sqrt{\frac{3}{5}} R_0 \cdot g(\varepsilon, \varepsilon_4)\,, \tag{3}$$

where the function g describes the dependence of the mean square radius on deformation. The equilibrium deformations of nuclei were taken from Ref. [5], where the two-dimensional (ε, ε_4) space of deformation parameters was used. The potential energy surfaces were calculated in Ref. [5] by the Strutinsky prescription with the zero–point energy correction terms according to the generator coordinate method [6].

Lateron it was found, after more broad calculations with the equilibrium deformations taken from Ref. [7], that the additional term $\sim \frac{1}{A}$ in the formula (2) should appear when reproducing the mean square radii of all nuclei beginning from the lightest ones up to the actinides [8]

$$r_0^{ch} = 1.240 \left(1 - 0.191 \cdot \frac{N-Z}{A} + 1.646 \cdot \frac{1}{A}\right) \text{ fm}\,. \tag{4}$$

A further development of the formula for nuclear radius was made in Ref. [9] after extensive Hartree-Bogolubov calculations with various sets of Skyrme effective interactions for proton and neutron density distributions in a few spherical nuclei. The authors of Ref. [9] postulate new terms proportional to $1/A^2$ in the formula for r_0^{ch}.

The aim of our present work is to find simple formulae which approximate the results obtained for proton and neutron radii within the RMFT [10, 11]. We investigate all even-even β stable nuclei as well as the isotopes and isotones corresponding to major magic Z and N numbers. When discussing the nuclides far from stability we change the mass number A up to the zero neutron or proton separation energy.

In Section 2 we describe briefly the theoretical model and its parameters. In Section 3 we analyze the results of the calculations and we write formulae for the radii of the proton and neutron distributions, which approximate the theoretical results of the RMFT. A simple, phenomenological formula for neutron radii is proposed as the result of the above analysis. The conclusions and further investigations perspectives are described in Section 4.

2 Theoretical model

The relativistic mean field theory [10] is a variational model based on a standard Lagrangian density [11]

$$\begin{aligned}\mathcal{L} &= \bar{\psi}_i \left[\gamma^\mu (i\partial_\mu - g_\omega \omega_\mu - g_\rho \vec{\rho}_\mu \vec{\tau} - e\frac{1-\tau_3}{2} A_\mu) - M - g_\sigma \sigma\right] \psi_i \\ &+ \frac{1}{2}(\partial\sigma)^2 - U(\sigma) - \frac{1}{4}\Omega_{\mu\nu}\Omega^{\mu\nu} + \frac{1}{2} m_\omega^2 \omega^2 \\ &- \frac{1}{4}\vec{R}_{\mu\nu}\vec{R}^{\mu\nu} + \frac{1}{2} m_\rho^2 \vec{\rho}^2 - \frac{1}{4} F_{\mu\nu} F^{\mu\nu} \ ,\end{aligned} \tag{5}$$

consisting of nucleon ψ, mesons $\sigma, \omega, \vec{\rho}$ and electromagnetic $\vec{A}$ fields. The σ mesons potential has been taken in the nonlinear form:

$$U(\sigma) = \frac{1}{2} m_\sigma^2 \sigma^2 + \frac{1}{3} g_2 \sigma^3 + \frac{1}{4} g_3 \sigma^4 \ . \tag{6}$$

It was found in [12] that the NL-3 [13] parameters set of the mean field Lagrangian (5) reproduced well binding energies, proton and neutron separation energies, electric quadrupole moments and radii of all nuclei along the whole β–stability line. The NL-3 parameters are:

– nucleon mass	$M = 939$ MeV
– meson masses	$m_\sigma = 508.194$ MeV, $m_\omega = 782.501$ MeV, $m_\rho = 763$ MeV
– meson coupling constants	$g_\sigma = 10.217$, g_ω= 12.868, $g_\rho = 4.474$
– σ meson field constants	g_2 = –10.431 1/fm, g_3= -28.885

The relativistic Hartree equations are solved by iterations: one starts with some estimate of the meson and electromagnetic fields, then solving the Dirac equation one finds the Dirac spinors. They give the densities and currents as sources for the Klein-Gordon equations for the meson fields. After their solution the new set of the meson and electromagnetic fields is found as the starting point for the next iteration. When the selfconsistency is achieved, Hartree-Bogolubov wave functions $\Psi^{p(n)}$ of protons and neutrons are used for evaluation of the mean values of operators in interest. We assume here the product of the BCS–type functions

$$|\Psi\rangle = \prod_{\nu>0} (u_\nu + v_\nu a_\nu^+ a_{-\nu}^+)|vac\rangle \tag{7}$$

for protons and neutrons as the ground state wave function of nucleus.

To get the strength of the pairing interaction for nuclei from very different regions, we have taken simply the experimental energy gaps (Δ) and the lowest in energy Z (or N) single–particle levels when solving the BCS equations. Such a procedure is justified in our calculations because the quantities which we evaluate depend rather weakly on the choice of the pairing force. All Δ–s are extracted from the experimental mass differences

taken from the Wapstra–Audi tables [14] but for the isotopes for which the experimental data do not exists we have used the estimates: $\Delta_{p(n)} = 12/\sqrt{A}$ MeV.

The monopole moments of protons and neutrons distributions are

$$Q_0^{p(n)} = \langle\Psi| \sum_\nu r_\nu^2 |\Psi\rangle^{p(n)} \,. \tag{8}$$

The mean square radii (MSR) are defined

$$\langle r^2\rangle_p = \frac{Q_0^p}{Z} \,, \qquad \langle r^2\rangle_n = \frac{Q_0^n}{N} \,. \tag{9}$$

and the root mean square radii (RMSR) are

$$r_{p(n)} = \sqrt{\langle r^2\rangle_{p(n)}} = \sqrt{\frac{3}{5}} R_{p(n)} \,. \tag{10}$$

In equations (9–10) we have neglected corrections originating from the center of mass motion. For heavier nuclei which we discuss these corrections are small. The quadrupole moments of proton and neutron distributions are given by

$$Q_2^{p(n)} = \langle\Psi| \sum_\nu 2r_\nu^2 \, P_2(\cos\vartheta_\nu) |\Psi\rangle^{p(n)} \,, \tag{11}$$

where P_2 is the Lagrange polynomial of the order 2. The quadrupole deformation parameter of proton or neutron distribution is approximately equal to

$$\beta_2^{p(n)} \approx \sqrt{\frac{4\pi}{5}} \frac{Q_2^{p(n)}}{Q_0^{p(n)}} \,. \tag{12}$$

We have evaluated also the binding energies of nuclei ($B_{\rm RMF}$), the reduced electric quadrupole transition probabilities ($B(E2)$), the proton and neutron separation energies ($S_{p(n)}$). The results are compared with the experimental data taken from Refs. [1, 2, 14].

3 Results

Various functions of radii and density moments were investigated in order to extract the isospin dependence of proton and neutron density distributions. The calculations were performed for the stable nuclei along the β stability line and for all potentially existing isotopes with Z=50, 56, 82, 94 and isotones with N=50, 82, 126. Schematic view in the (N, Z) plane of the nuclides discussed in the paper is presented in Fig. 1. For the nuclei out of β–stability line the calculation was made until the proton or neutron drip line was reached.

In Fig. 2 the set of results concerning the β-stable nuclei with $40 \leq A \leq 256$ is presented as a function of mass number A. For each A value only one isotope with the smallest mass is chosen.

The upper left figure shows the difference between the binding energy $B_{\rm RMF}$ of a nucleus calculated by the RMFT with the NL-3 parameters set and its experimental value $B_{\rm exp}$ taken from [14]. Here the maximal error of the RMFT estimates is 5 MeV only (for $A = 150$).

The upper right figure presents the reduced electric quadrupole transition probabilities $B(E2)$ obtained by the RMFT (solid line) compared to the experimental data [1] (circles). The agreement is rather good in spite of too large theoretical predictions of the nuclei about $A \sim 170$ and 250.

The separation energies of neutron S_n (left hand side) and proton S_p (right hand side) evaluated within the RMFT agree with the experimental data [14] (circles) very well.

The neutron r_n and proton r_p root mean square radii calculated by the RMFT presented in the lowest left hand side figure are also close to the experimental data (crosses for protons [1] , circles for neutrons [2]). The both radii are slightly different from each other, what is connected with the different in size and in deformation proton and neutron density distributions.

The difference of the proton and neutron quadrupole deformations obtained in the RMFT calculation is shown in the lowest right part of Figure 2. One can see that for same nuclei it exceeds 0.03.

The next seven figure sets (Figs. 3-9) show similar results as in Fig. 2 but for the isotope and isotone chains presented in Fig. 1. The experimental data (crosses for protons, circles for neutrons) are drawn, if they exist. The results should illustrate the goodness of the RMFT also for the nuclei outside β stability line. Using these results we can extract the isospin dependence of proton and neutron radius constants.

In Fig. 3 the same quantities as in Fig. 2 for Sn isotopes with $N = 50-86$ are drawn. All Sn nuclei are almost spherical so the quadrupole deformation of proton and neutron distribution is 0 (lowest right hand side picture). Also the reduced electric quadrupole transition probabilities $B(E2)$ proportional to the square of quadrupole moment are zero in the theory and the experiment as well (upper right hand side picture). The results both for proton and neutron radii are well confirmed by the experimental data what can be seen in the lowest left figure. The RMFT radii of neutron and proton distributions differ from each other up to 0.5 fm for the heaviest isotopes. The experimental separation energies are very well reproduced by the RMFT calculation (middle pair of figures). The binding energies obtained by the RMFT differ only up to 2.5 MeV from the experimental ones (upper left hand side picture).

The Ba isotopes presented in Fig. 4 are slightly deformed. One can see in the lower right figure that the neutron and proton deformations are slightly different. The RMFT reproduces the experimental kink in neutron separation energy S_n around neutron magic number ($N = 82$)

The Pb isotopes are presented in Fig. 5. The equilibrium deformations are largest for he isotopes around $A = 195$. The proton and neutron radii differ from each other much especially for the lighter isotopes. Unfortunately the RMFT estimate of the neutron root mean square radius for ^{208}Pb is pretty far from the experimental value [2].

The Pu isotopes, shown in Fig. 6 behave quite regularly in spite of the relative large deformations and $B(E2)$. The quadrupole deformations of proton and neutron distributions differ by about 0.025 for all isotopes. This difference is about 10 % of the average deformation of these nuclei.

In spite of the constant Z values the proton radius in Sn, Ba and Pb isotopes grows with the neutron number. It is not the case for the isotones shown in the next 3 figures: 7–9, where the neutron radii stay almost constant when number of protons Z grows.

In Fig. 7 the $N = 50$ spherical isotones (Ni-Sn) are presented. The errors in the binding energy are rather small. Due to the spherical shape of these nuclei no differences in proton and neutron deformations are observed. Contrary to the neutron radius the proton radius grows here rapidly with A.

Also the $N = 82$ isotones (Cd-Hf) shown in Fig. 8 have an almost constant neutron density distribution radius. This conclusion is also confirmed by the results presented in Fig. 9, for $N = 126$ isotones of Hg-U.

In order to extract the average isospin dependence of the radius constant from the root mean square radii evaluated within the RMFT we have divided the RMSR values by the factor $\sqrt{3/5}A^{1/3}$ (see Eq. 10). As one can see in Figs. 10a and 10b the radius constants of protons (crosses) and neutrons (circles) are gathered around 1.25 fm and 1.20 fm respectively as functions of the relative neutron excess $I = (N - Z)/A$. In order to analyze better the results one has to remove the influence of deformation on nuclear radii. We have renormalized them to the sphere using the volume conservation rule. It was made approximately by dividing the nuclear radii constants by factor g:

$$g\left(\beta_2\right) = 1 + \frac{5}{4\pi}\beta_2^2 \,. \tag{13}$$

This renormalized quantities $R_0 = r/(\sqrt{3/5} \cdot g(\beta_2))$ are shown on Fig. 10a, b for Ba and Pb isotopes respectively. Now one can see that the renormalized proton radii (diamonds) decrease almost linear with I while the neutron ones (dots) increase.

The above investigation has convinced us that the microscopic radius constant $r_0^{p,n}$ must depend also on the isospin I. The additional dependence on $1/A$ was noticed when comparing the results for different isotope chains. In Figs. 11, 12 the results are shifted by the terms proportional to $1/A$ in order to see better the average I dependence of the radii.

In Fig. 11 we present the proton and in Fig. 12 the neutron renormalized radii constant for all the isotope and isotone chains discussed in this paper (a) and for the β-stable nuclei (b). The results for protons are shifted by the term $0.8/A$ fm while the neutron estimates by $-3.3/A$ fm.

The dashed lines present average behavior of calculated radii constants. It was found by minimization of the mean square deviations. The following formulae for proton and neutron radii:

$$R_0^p = 1.237\left(1 - 0.157 \cdot \frac{N-Z}{A} - 0.646 \cdot \frac{1}{A}\right) A^{1/3} \text{ fm}$$

and (14)

$$R_0^n = 1.176\left(1 + 0.250\cdot\frac{N-Z}{A} + 2.806\cdot\frac{1}{A}\right)A^{1/3}\ \text{fm}$$

approximate the results obtained within the RMFT with the NL-3 set of the parameters. One can believe that the parameters of these formulae, found for the representative nuclei all over the periodic system can describe well the average trend of the results obtained within the RMFT.

The following formula approximates the RMFT results for the nuclear charge radii:

$$R_0^{ch} = 1.241\left(1 - 0.154\cdot\frac{N-Z}{A} + 0.580\cdot\frac{1}{A}\right)A^{1/3}\ \text{fm}\,. \tag{15}$$

This equation, obtained only by the analysis of the RMFT calculation results, has not much different parameters to those from equation (3) fitted to all available experimental data. The coefficient of $(N-Z)/A$ term is only slightly smaller than in the phenomenological formula (3). But the parameter at the term $1/A$ in (15) is almost 3 times smaller than in Eq. (3). It is mostly due to the fact that we have analyzed the nuclei with $A \geq 40$ while the Eq. (3) was obtained by fitting the experimental data for all nuclei with $A \geq 12$.

From Figs. 11 and 12 we can learn that the average formulae (14) work properly only for nuclei with $A \geq 60$. Also some nuclei with $I \sim 0.2$ don't fit to the average formulae. It is caused by non quadrupole deformations (octupole?) of these nuclei which were not included in the present analysis.

As far as the ratio of proton to neutron radii (or RMSR) is concerned there is almost no influence of deformation on the results. It is caused by the similar or identical shapes of proton and neutron density distributions. We have found a short formulae for this ratio similar to those for radii constants (14,15). The dependence of proton to neutron radii ratio on I is shown in Fig. 13. We have shifted the ratio by the term $-3.3/A$ in order to remove the influence of the $1/A$ dependence. Dashed lines in Fig. 13 represent the formula:

$$\frac{r_p}{r_n} = 1.048\left(1 - 0.364\cdot\frac{N-Z}{A} - 3.148\cdot\frac{1}{A}\right) \tag{16}$$

fitted by the least square fit to the r_p/r_n RMFT ratios for all nuclides shown Fig. 1. In Fig. 13a the radii ratios of these chains of isotopes and isotones are presented while in Fig. 13b the corresponding results for β-stable nuclei with $A \geq 40$ are plotted. The results for nuclei with $A \geq 60$ from are reproduced well by formula (16).

Eq. (16) can be used to estimate the neutron RMSR from the charge one. It could be useful because it exists over 250 measured charge RMSR and only few experimental ones for the neutron RMSR. One can rearrange Eq. (16) using the relation between the charge and proton mean square radii

$$r_{ch}^2 = r_p^2 + 0.64\ \text{fm}^2\,. \tag{17}$$

The term 0.64 fm^2 originates from the final size of the proton. Finally one gets:

$$r_n = \frac{(r_{ch}^2 - 0.64)^{1/2}}{1.048\,(1 - 0.364\cdot(N-Z)/A - 3.148/A)}\ \text{fm}\,. \tag{18}$$

In Fig. 14 all known experimental RMSR (errorbars) [2] for neutrons are compared with the RMFT predictions (crosses) and with the results estimated from experimental charge RMSR [2] using Eq. (18) (circles). All results agree very well with each other, so we hope that the formula (18) can be used by the experimentalists to foresee the neutron distribution radii for other nuclei as well.

4 Conclusions

The following conclusions can be drawn from our calculation

1. The renormalized to sphere RMFT proton and neutron distributions radii $R_0^{p(n)}$ depend almost linear on neutron excess $I = (N - Z)/A$. R_0^p decrease with I, while R_0^n increase what was suggested in [8] and obtained in [9] by the analysis of the results obtained within the HFB calculation with the Skyrme forces.

2. The parameters of the formulae for the charge radii are similar as in the phenomenological formula in [8]. However the dependence of the RMFT radii on I is about 20% weaker than in the phenomenological formula which describes the global experimental trend. It means that the parameters NL-3 of the RMFT should be slightly changed.

3. The term $\sim A^{-1}$ in the formula for $R_0^{p(n)}$ is needed in order to reproduce the average MSR values obtained within the RMFT. Its role is especially important for lighter nuclei.

4. The ratio of the proton radius to the neutron radius is a smooth function of I and A^{-1} and it could be very well described by the simple formula (16). Using this global dependence we have written the phenomenological formula (18) which allows to foresee the magnitude of the neutron radius when the experimental charge radius is known. The prediction power of the formula (18) is not worse than that of very advanced microscopical calculations based on the RMFT or the HFB-Skyrme model [9].

The obtained formulae for the R_0^n and R_0^p radii will be used to develop the liquid drop like model, which will depend on the different proton and neutron density distributions, i.e. different radii and deformations. Such investigations are in progress now [15].

Acknowledgment:

The authors gratefully acknowledge the helpful discussions with Peter Ring and offering by him the numerical code for solving the relativistic Hartree model.

References

[1] E. W. Otten, Treatise on heavy ion science, Vol. **8**, Bromley D. A. (Ed.), New York, Plenum Press, (1989) 517.

[2] C. J. Batty, E. Friedman, H. J. Gils, H. Rebel, At. Data and Nucl. Data Tables **36** (1987) 49.

[3] A. Bohr, B. Mottelson, Nuclear structure, Vol. 1, W. A. Benjamin Inc., New York, Amsterdam, (1969).

[4] B. Nerlo-Pomorska, K. Pomorski, Z. Phys. **A344** (1993) 359.

[5] B. Nerlo-Pomorska, B. Mach, At. Data and Nucl. Data Tables **60** (1995) 287.

[6] B. Nerlo-Pomorska, K. Pomorski, B. Mach, Nucl. Phys. **A562** (1993) 180.

[7] P. Möller, J. R. Nix, W. D. Myers, W. J. Swiatecki, At. Data and Nucl. Data Tables **59** (1995) 185.

[8] B. Nerlo-Pomorska, K. Pomorski, Z. Phys. **A348** (1994) 169.

[9] J. Dobaczewski, W. Nazarewicz, T. R. Werner, Z. Phys. **A354** (1996) 27.

[10] B. D. Serot and J. D. Walecka, Adv. Nucl. Phys. **16** (1997) 1.

[11] P. Ring, Prog. Part. Nucl. Phys. **37** (1996) 193.

[12] K. Pomorski, P. Ring, G. A. Lalazissis, A. Baran, Z. Łojewski, B. Nerlo-Pomorska, M. Warda, Nucl. Phys. **A624** (1997) 329.

[13] G. A. Lalazissis, H. M. Sharma, P. Ring, Y, K. Gambhir, Nucl. Phys. **A508** (1996) 202.

[14] G. Audi, A. H. Wapstra, Nucl. Phys. **A595** (1995) 409.

[15] K. Dietrich, B. Nerlo-Pomorska, K. Pomorski, in preparation.

Figure captions

1. Schematic view in the (N, Z) plane of the nuclides discussed in the paper. For the nuclei out of the β-stability line the calculation was made until the proton or neutron drip line was reached.

2. The results obtained within the RMFT+BCS model with the NL-3 parameters [13] for the β-stable nuclei compared with the experimental data as a functions of mass number A. In the diagrams are presented: the difference between the calculated $B_{\rm RMF}$ and experimental $B_{\rm exp}$ binding energy (upper-left figure), reduced electric quadrupole transition probabilities $B(E2)$ (upper-right figure), neutron and proton separation energies S_n, S_p (middle figures), neutron and proton root mean square radii r_n, r_p (lower-left figure), differences between proton and neutron quadrupole deformation parameters $\beta_2^p - \beta_2^n$ (lower-right figure).

3. Same as in Fig. 2 but for the Sn isotopes ($Z = 50$).

4. Same as in Fig. 2 but for the Ba isotopes ($Z = 56$).

5. Same as in Fig. 2 but for the Pb isotopes ($Z = 82$).

6. Same as in Fig. 2 but for the Pu isotopes ($N = 94$).

7. Same as in Fig. 2 but for the isotones with $N = 50$.

8. Same as in Fig. 2 but for the isotones with $N = 82$.

9. Same as in Fig. 2 but for the isotones with $N = 126$.

10. The proton (crosses) and neutron (open circles) nuclear radii divided by $A^{1/3}$ as function of the relative neutron excess I for Ba (a) and Pb (b) isotopes. Nuclear radii renormalized to sphere are plotted with diamonds and dots respectively.

11. Renormalized to sphere proton radii constants for discussed chains of isotopes and isotones (a) and for all β stable nuclei with $A \geq 40$ (b) as function of the relative neutron excess I shifted down by the $-3.3/A$ fm term. Dashed line represents average behavior of calculated values for the chains (14).

12. Same as in Fig. 11 but for neutron radii (shifted up by the $0.8/A$ fm term).

13. The ratios of the proton to neutron root mean square radii for discussed chains of isotopes and isotones (a) and for the β stable nuclei with $A \geq 40$ (b) as functions of relative neutron excess I. The ratios are shifted up by $3.3/A$ fm term. Dashed lines represent the average behavior of calculated values (16).

14. Comparison of the experimental neutron root mean square radii [2] (errorbars) with the RMFT results (crosses) and the values obtained from experimental charge radii [2] through the new formula (18) (circles).

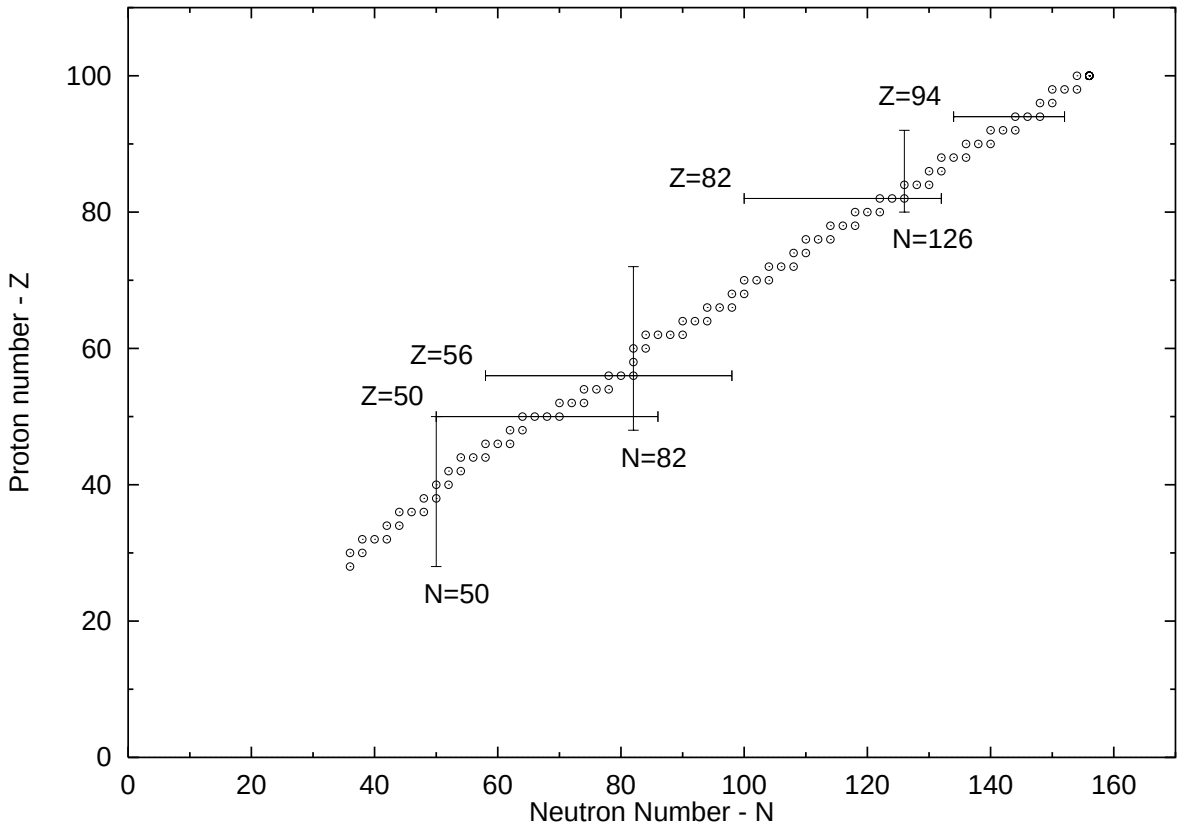
Proton number - Z
Neutron Number - N
0
20
40
60
80
100
120
140
160
0
20
40
60
80
100
Z=94
Z=82
N=126
Z=56
Z=50
N=82
N=50

Figure 1:

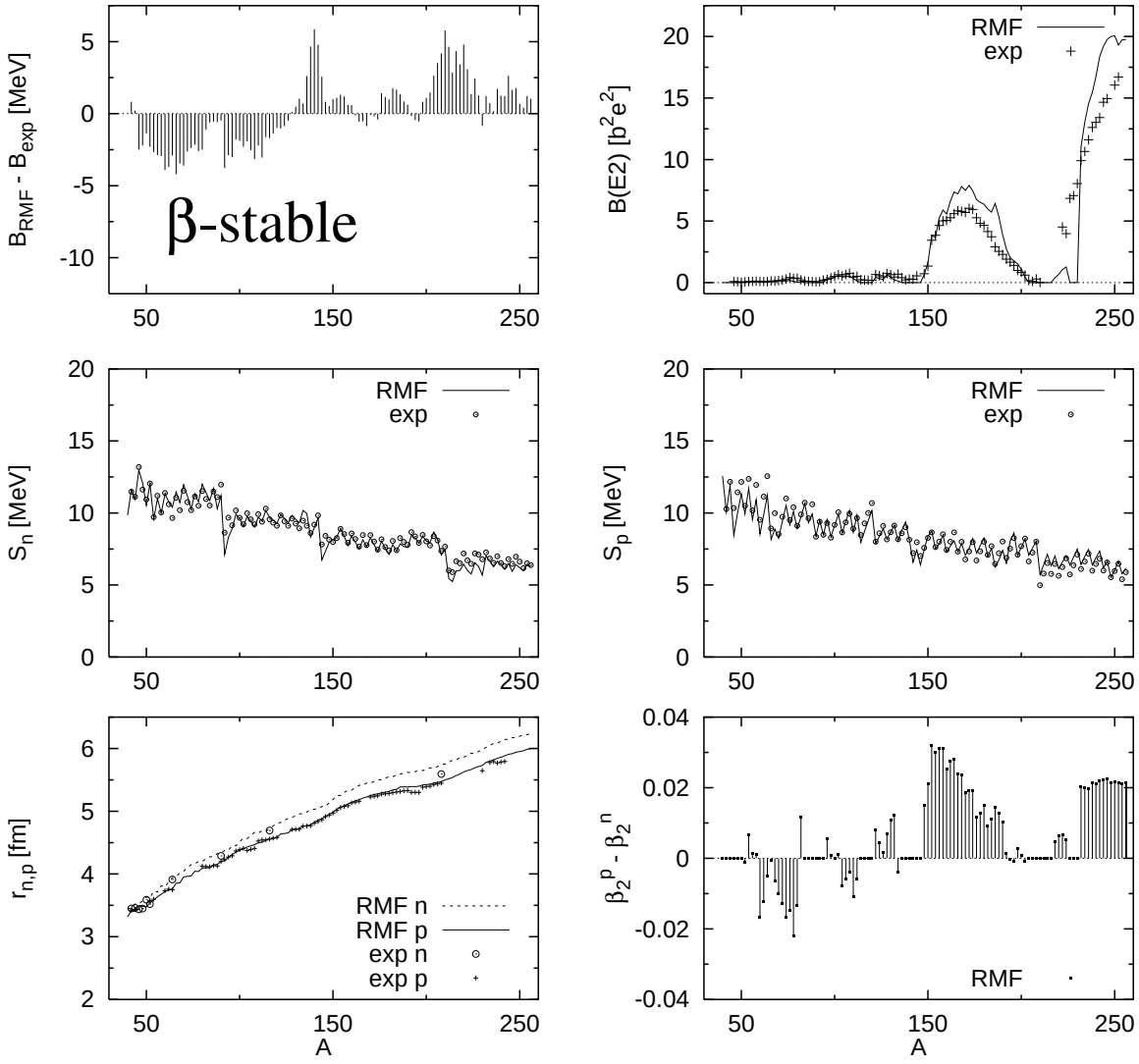

Figure 2:

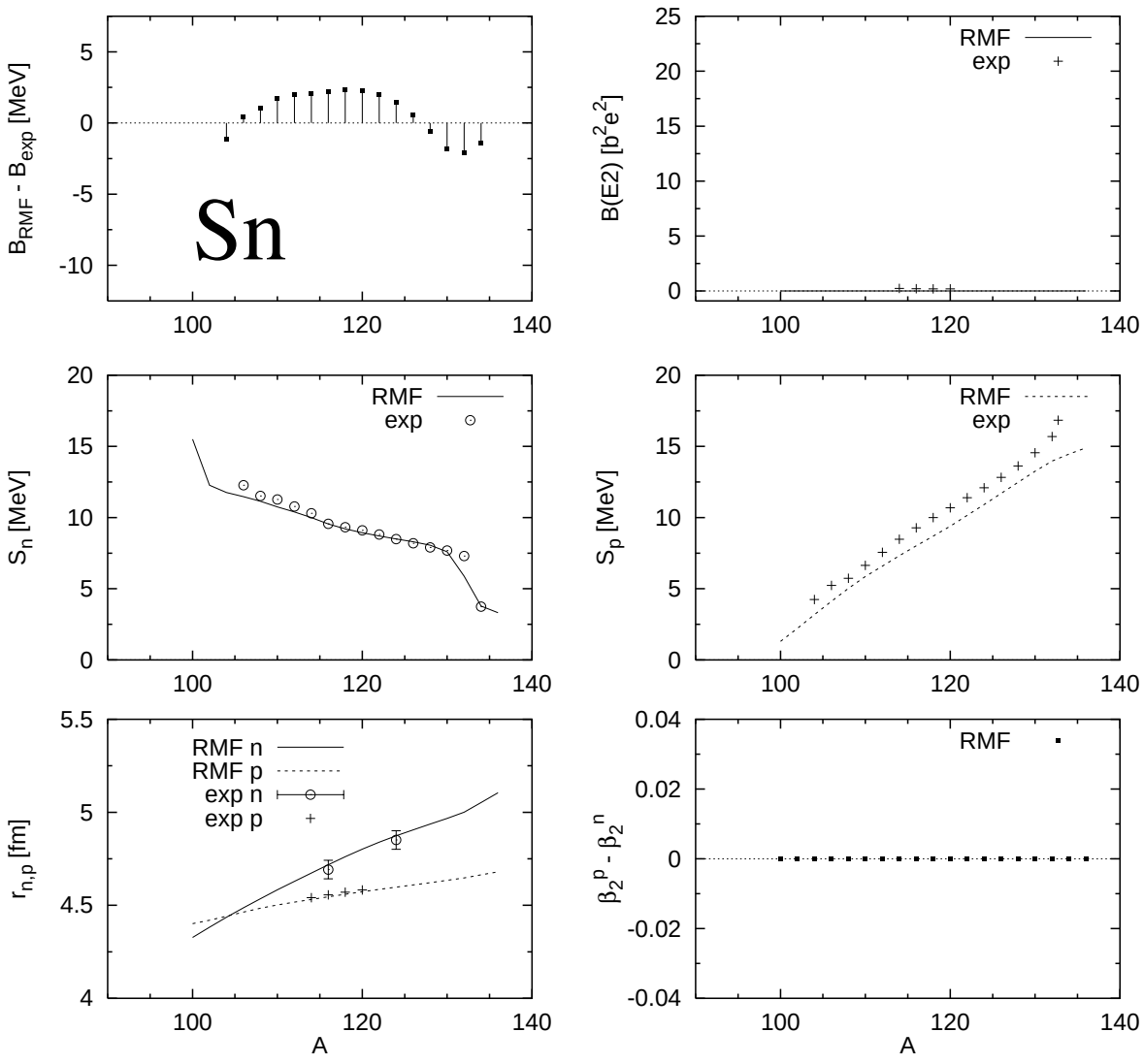
Sn
B_{RMF} - B_{exp} [MeV]
B(E2) [b^2e^2]
RMF
exp
S_n [MeV]
S_p [MeV]
RMF n
RMF p
exp n
exp p
$r_{n,p}$ [fm]
β_2^p - β_2^n
A

Figure 3:

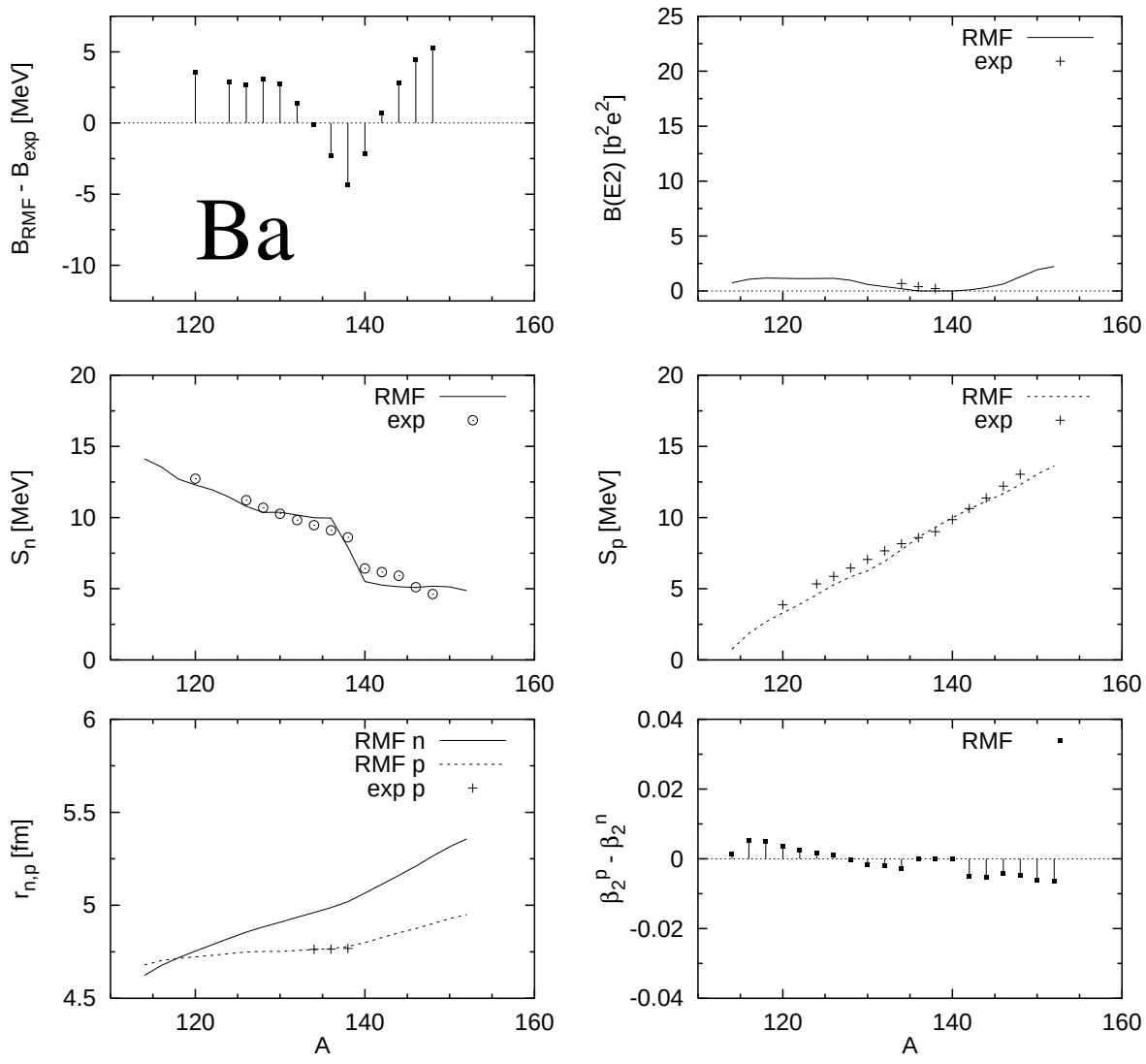
Ba
B_{RMF} - B_{exp} [MeV]
B(E2) [b^2e^2]
RMF
exp
S_n [MeV]
S_p [MeV]
RMF n
RMF p
exp p
$r_{n,p}$ [fm]
β_2^p - β_2^n
A

Figure 4:

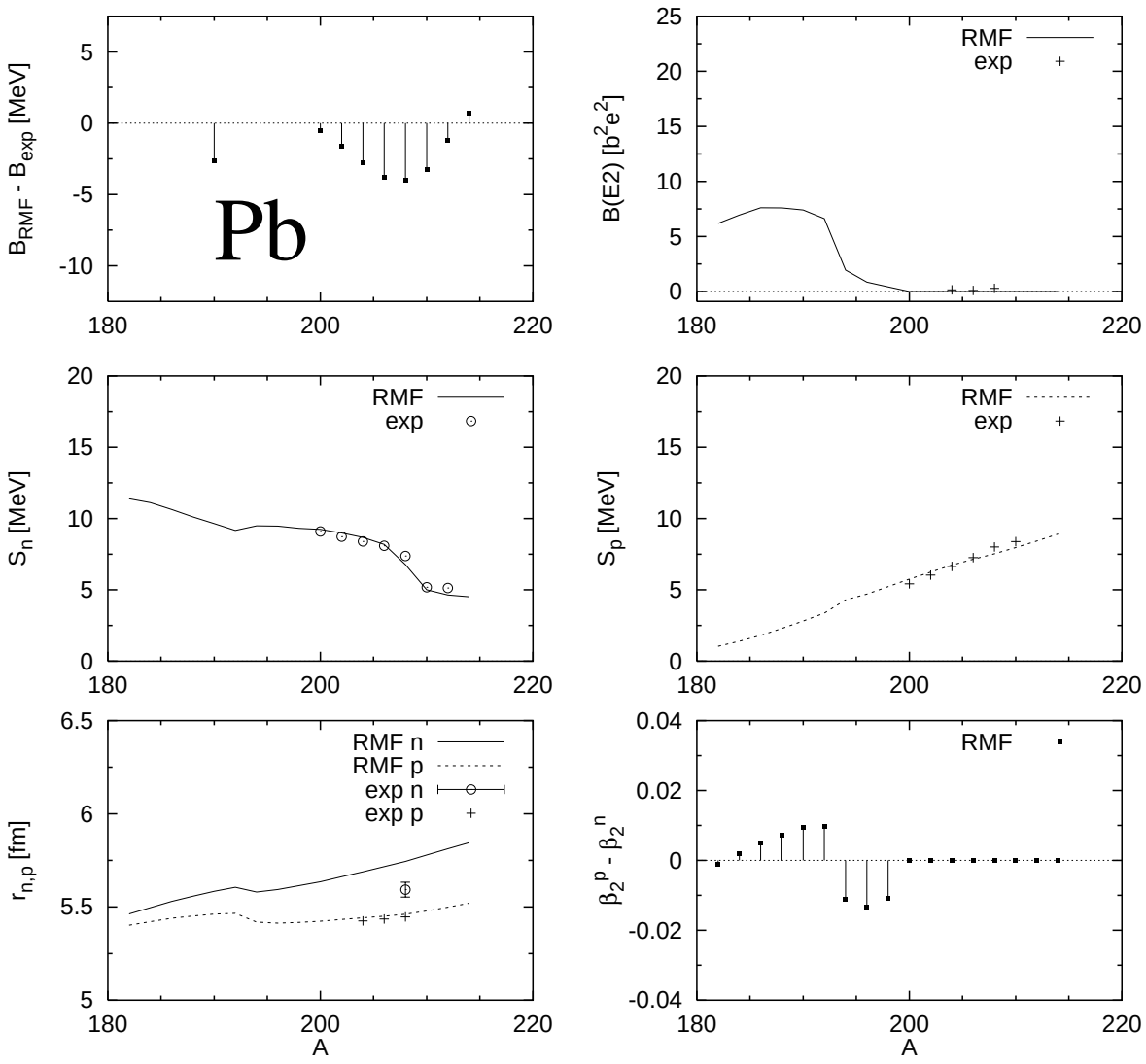
Pb
$B_{RMF} - B_{exp}$ [MeV]
B(E2) [b^2e^2]
RMF
exp
S_n [MeV]
S_p [MeV]
$r_{n,p}$ [fm]
RMF n
RMF p
exp n
exp p
$\beta_2^p - \beta_2^n$
A

Figure 5:

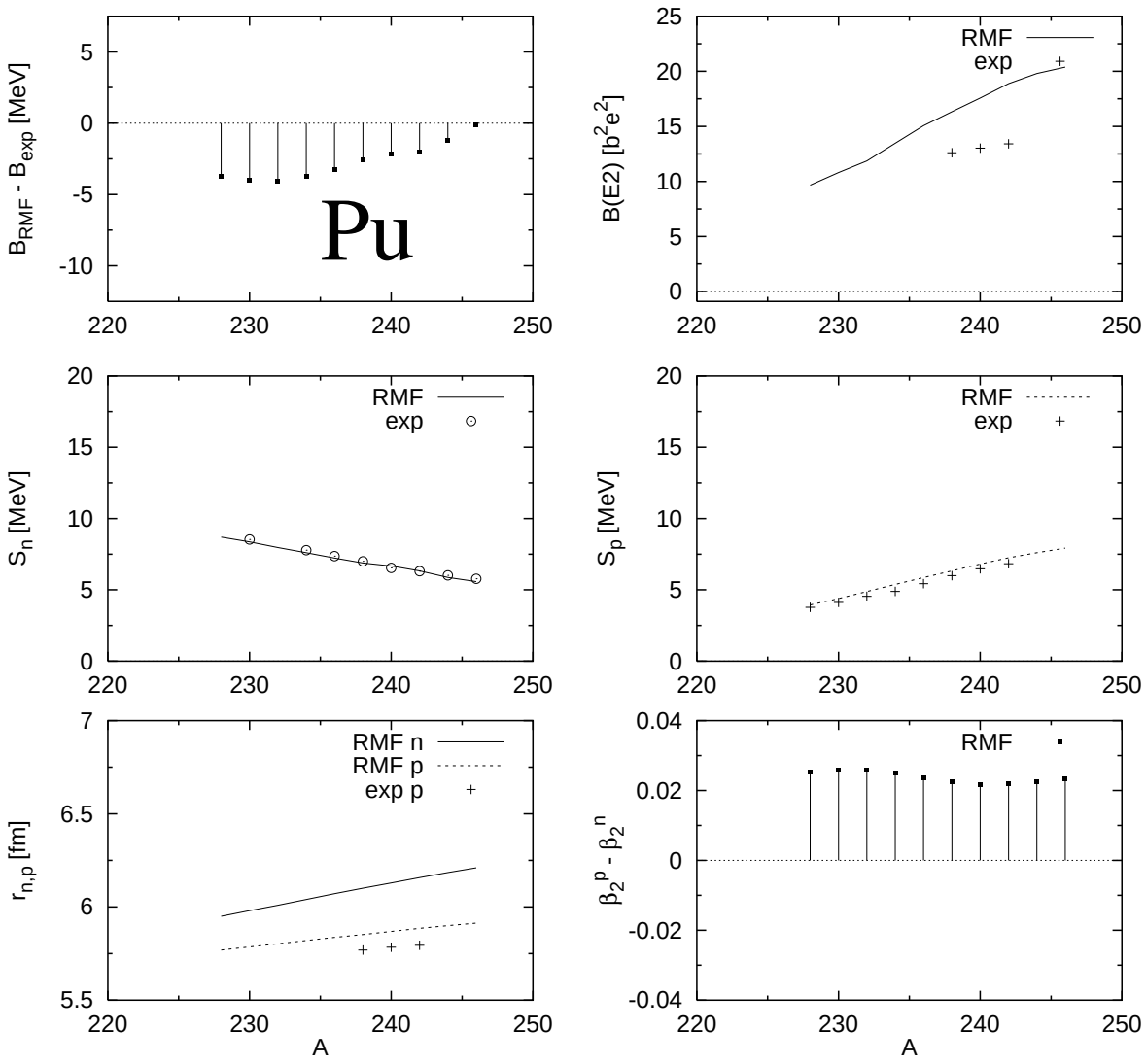
Pu
B_{RMF} - B_{exp} [MeV]
B(E2) [b^2e^2]
RMF
exp
S_n [MeV]
S_p [MeV]
RMF n
RMF p
exp p
$r_{n,p}$ [fm]
β_2^p - β_2^n
A

Figure 6:

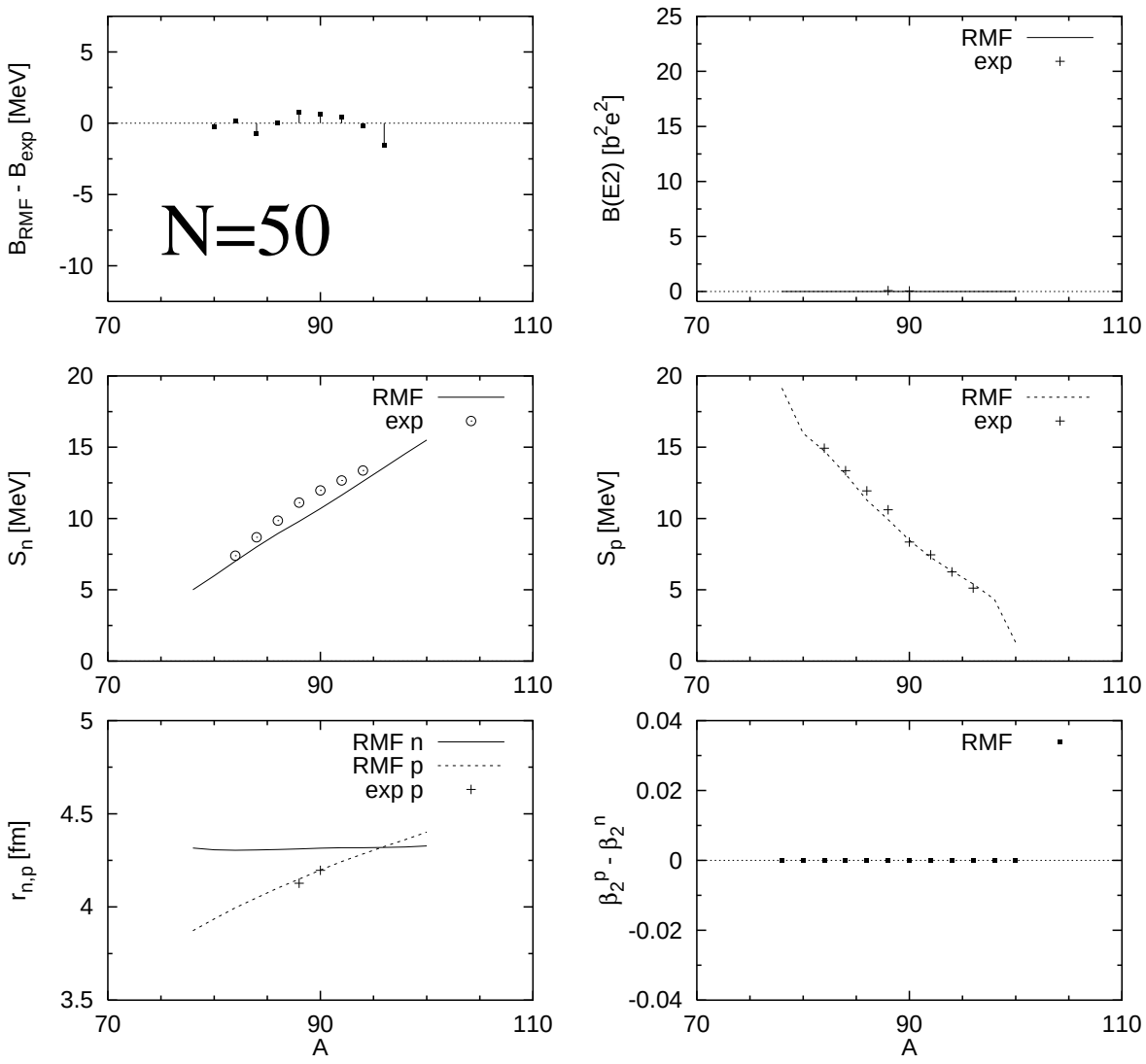
N=50
B_{RMF} - B_{exp} [MeV]
B(E2) [b^2e^2]
RMF
exp
S_n [MeV]
S_p [MeV]
RMF n
RMF p
exp p
$r_{n,p}$ [fm]
β_2^p - β_2^n
A

Figure 7:

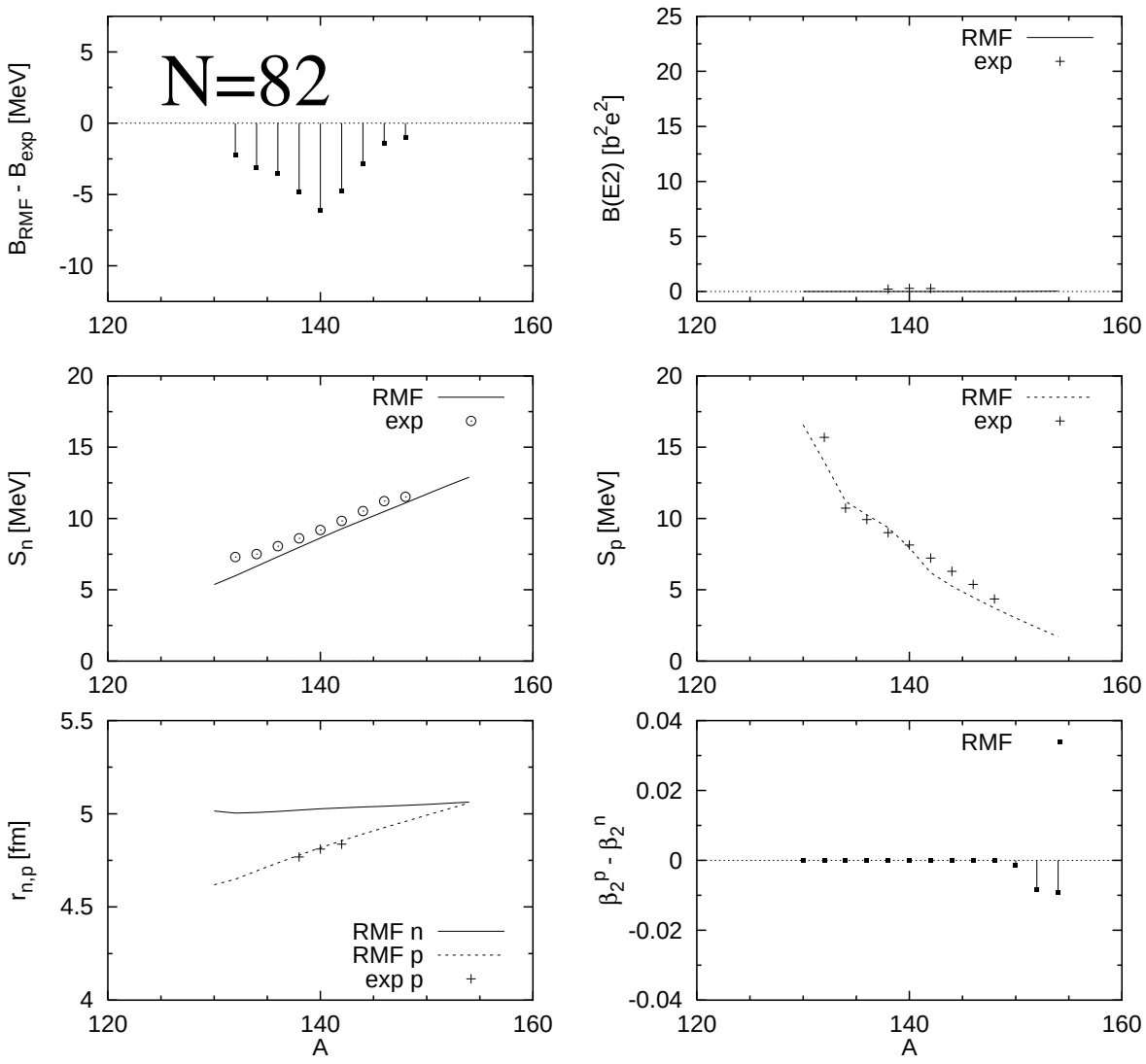
N=82
B_{RMF} - B_{exp} [MeV]
B(E2) [b^2e^2]
RMF
exp
S_n [MeV]
S_p [MeV]
$r_{n,p}$ [fm]
RMF n
RMF p
exp p
β_2^p - β_2^n
A

Figure 8:

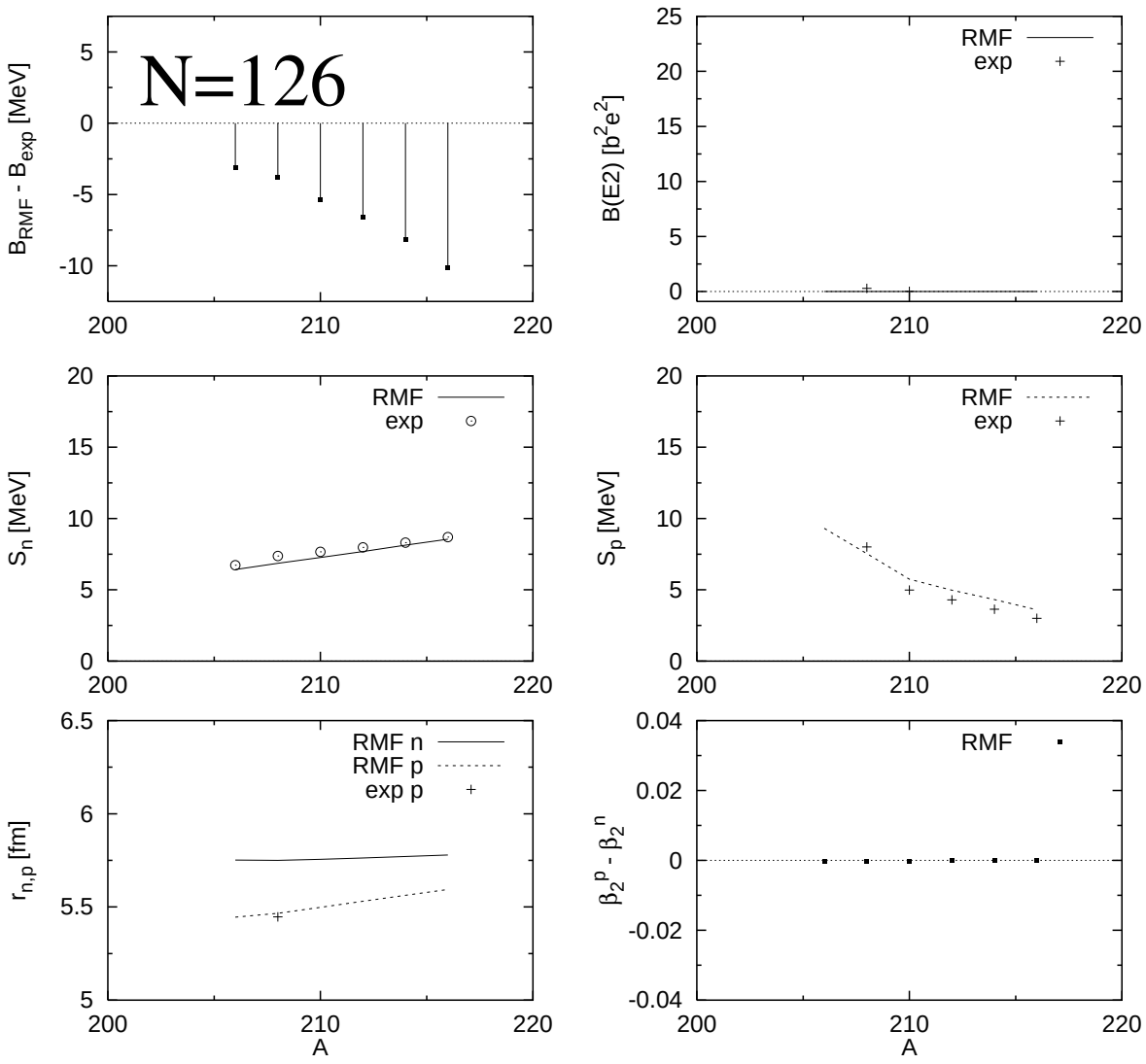
N=126
B_{RMF} - B_{exp} [MeV]
B(E2) [b^2e^2]
RMF
exp
S_n [MeV]
S_p [MeV]
RMF n
RMF p
exp p
$r_{n,p}$ [fm]
β_2^p - β_2^n
A

Figure 9:

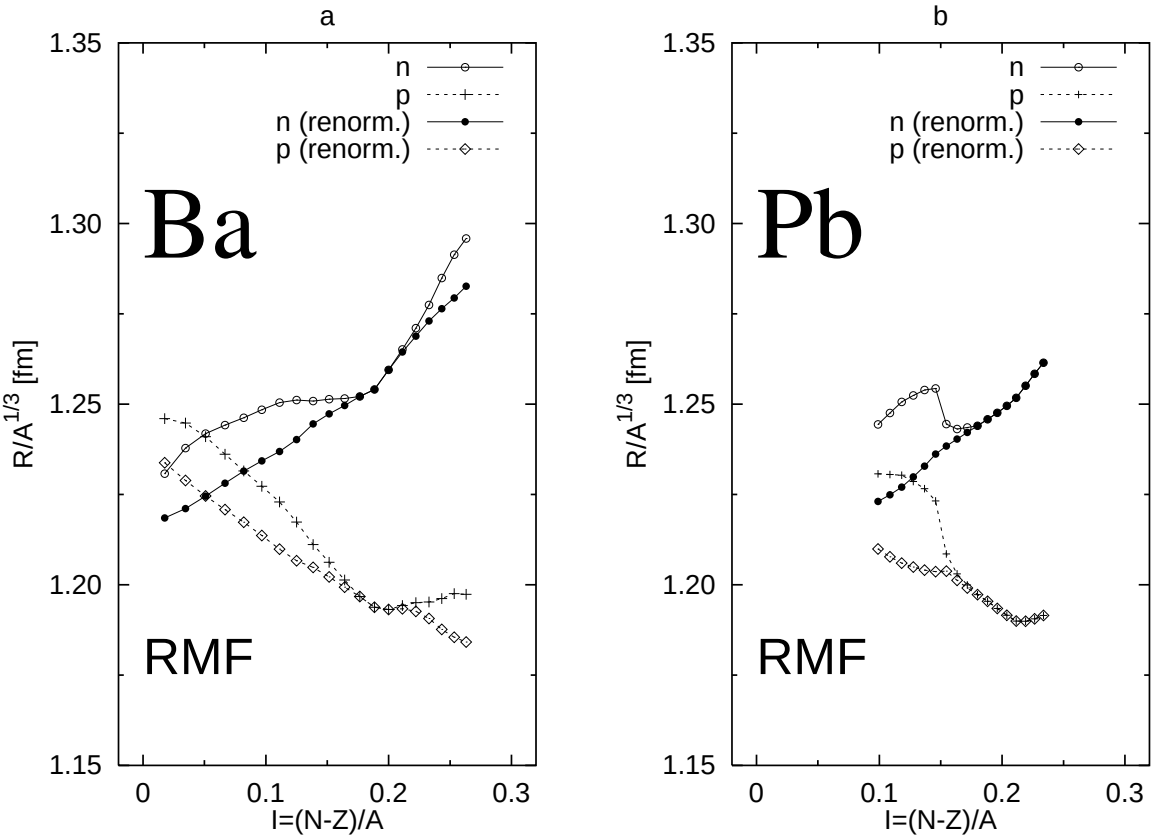
a
b
n
p
n (renorm.)
p (renorm.)
Ba
Pb
RMF
RMF
R/A^1/3 [fm]
I=(N-Z)/A
1.35
1.30
1.25
1.20
1.15
0
0.1
0.2
0.3

Figure 10:

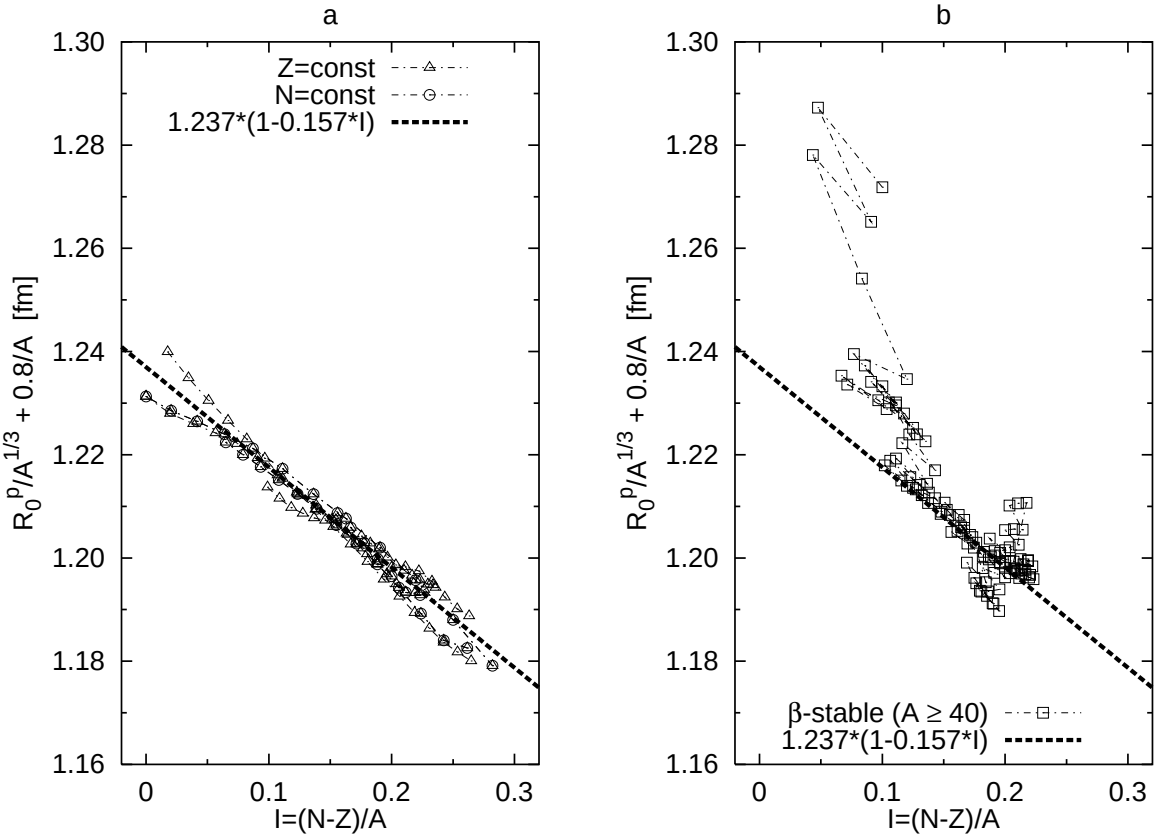
a
b
Z=const
N=const
1.237*(1-0.157*I)
β-stable (A ≥ 40)
1.237*(1-0.157*I)
$R_0^p/A^{1/3} + 0.8/A$ [fm]
I=(N-Z)/A
1.16
1.18
1.20
1.22
1.24
1.26
1.28
1.30
0
0.1
0.2
0.3

Figure 11:

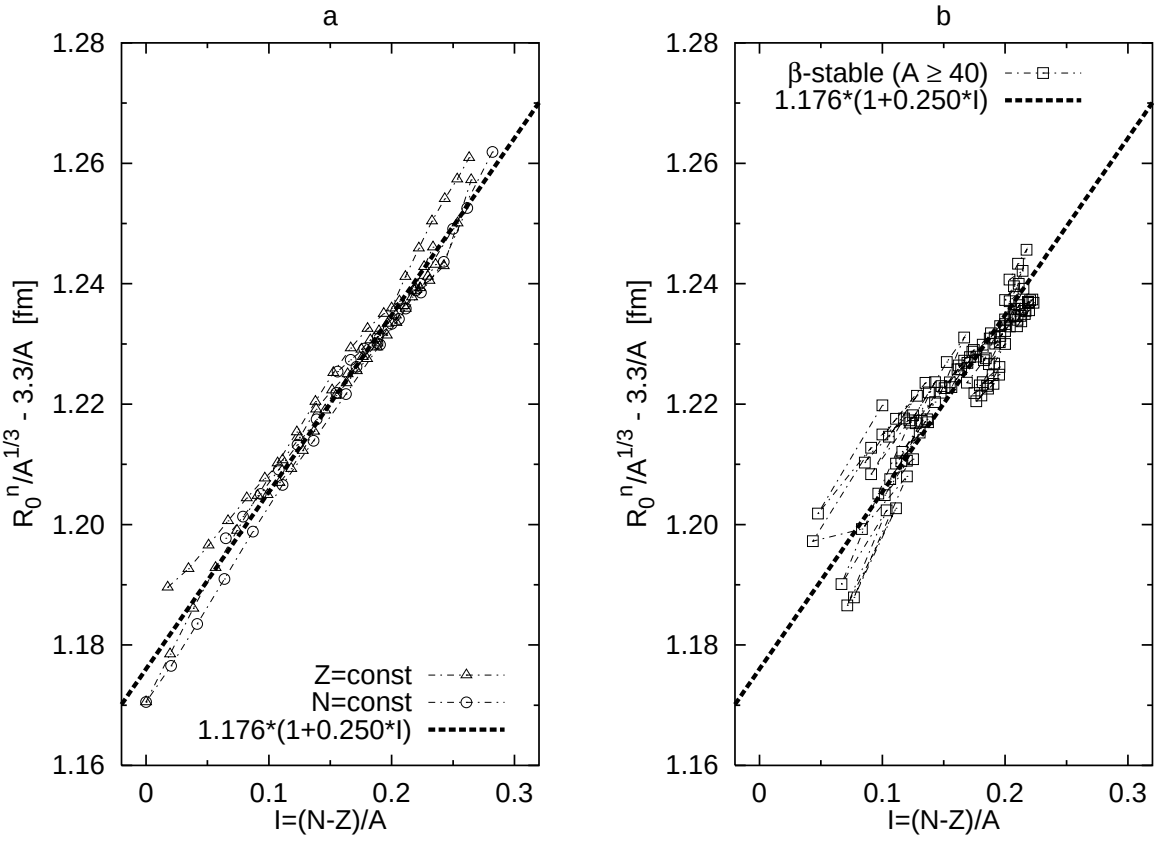
a
b
1.28
1.26
1.24
1.22
1.20
1.18
1.16
0
0.1
0.2
0.3
$R_0^n/A^{1/3}$ - 3.3/A [fm]
I=(N-Z)/A
Z=const
N=const
1.176*(1+0.250*I)
β-stable (A ≥ 40)
1.176*(1+0.250*I)

Figure 12:

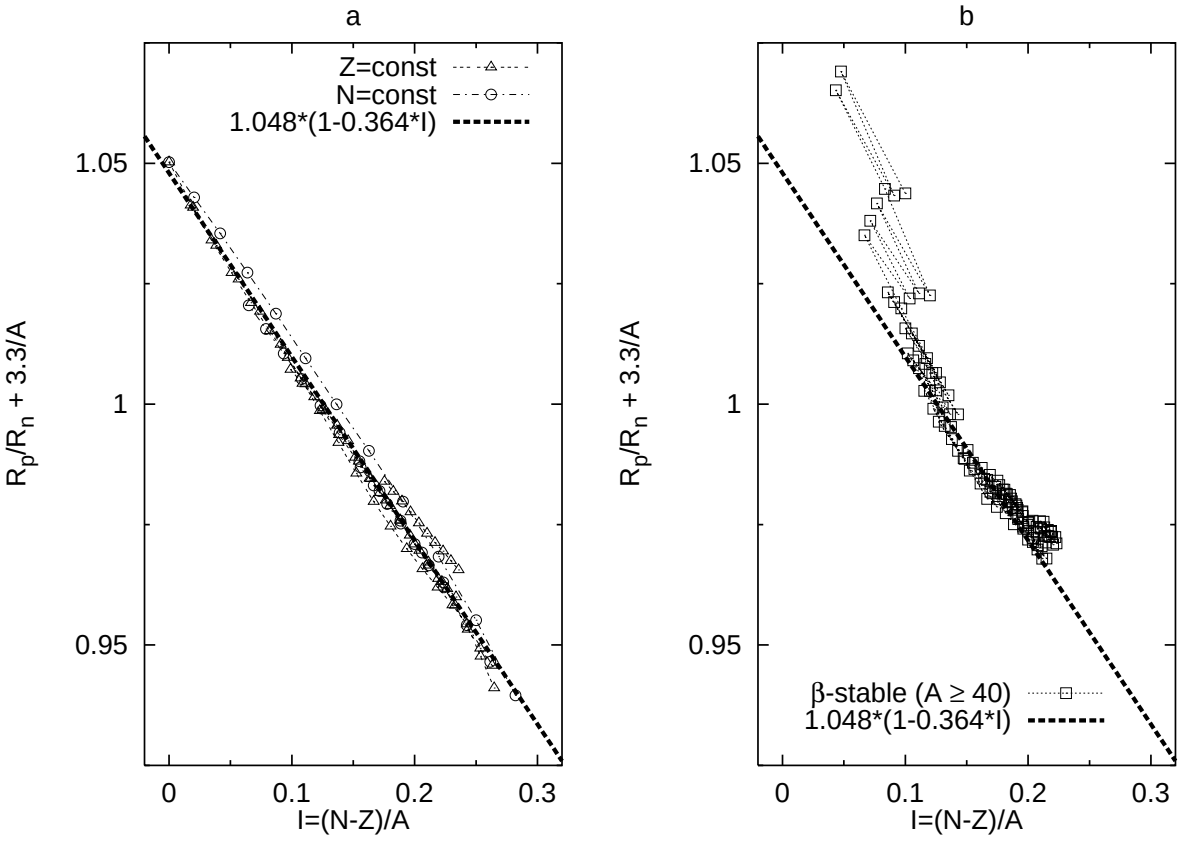
a
b
Z=const
N=const
1.048*(1-0.364*I)
β-stable (A ≥ 40)
1.048*(1-0.364*I)
R_p/R_n + 3.3/A
I=(N-Z)/A
1.05
1
0.95
0
0.1
0.2
0.3

Figure 13:

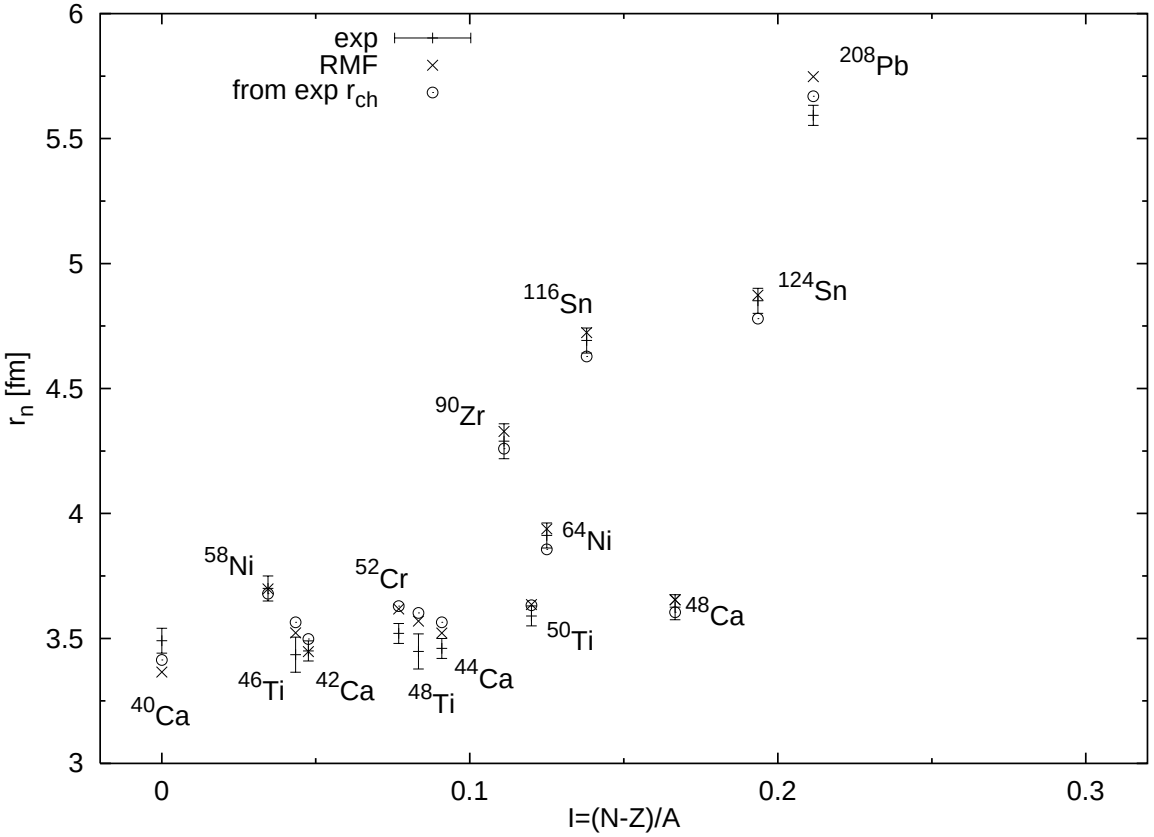
exp
RMF
from exp r_ch
208Pb
124Sn
116Sn
90Zr
64Ni
58Ni
52Cr
48Ca
50Ti
46Ti
42Ca
44Ca
48Ti
40Ca
r_n [fm]
I=(N-Z)/A
6
5.5
5
4.5
4
3.5
3
0
0.1
0.2
0.3

Figure 14: